ICE DETECTION IN SWISS LAKES USING MODIS DATA

Manu Tom, Charis Lanaras, Emmanuel Baltsavias, Konrad Schindler

ETH Zürich, Institute of Geodesy and Photogrammetry, Stefano-Franscini-Platz 5, 8093 Zürich, Switzerland
{manu.tom, lanaras, manos, schindler}@geod.baug.ethz.ch

KEY WORDS: Lake Ice, Semantic Segmentation, Climate Change, Super-Resolution, Satellite Images

ABSTRACT: In this research, we process low spatial resolution satellite images (MODIS) for integrated multi-temporal monitoring of ice in selected lakes in Switzerland. Lake ice is important for climate research and is considered one of the Global Climate Observing System's (GCOS) Essential Climate Variables (ECVs). The aim of our project is to detect whether a lake is frozen or not. Four of the target lakes are Sihl, Sils, Silvaplana and St. Moritz, showing different characteristics regarding area, altitude, surrounding topography and freezing frequency, describing cases of medium to high difficulty. From the satellite sensor MODIS with daily temporal resolution, several spectral channels are used, both reflective and emissive. The low-resolution MODIS bands with 500m and 1000m Ground Sampling Distance (GSD) are super-resolved to 250m resolution and co-registered prior to the analysis. Digitized lake outlines after generalization using Douglas Peucker Algorithm are back-projected on to the image space. As a pre-processing step, the absolute geolocation accuracy of the lake outlines is corrected by matching the projected outlines to the images. Only the cloud-free pixels which lie completely inside the lake (*clean pixels*) are analyzed. We formulate the lake ice detection as a two-class (frozen, non-frozen) semantic segmentation problem, but also analyze the three-class distinction where bare ice is separated from snow-covered ice, due to their different spectral properties. The most useful MODIS channels to solve the problem are identified with *xgboost*, while the classification is done with (non-linear) Support Vector Machines (SVM). The proposed method is tested on MODIS data from the cold winter 2011-12 and summer 2012 and we achieve >95% accuracy on all the four target lakes.

1. INTRODUCTION

(a) Lake Sihl (b) Lake Sils (c) Lake Silvaplana (d) Lake St. Moritz

Figure 1. Four target lakes in Switzerland (source: myswitzerland.com).

Inland water bodies, especially lakes, are of considerable importance in climate change research and global warming studies. Lake ice can indirectly offer hints on alterations in physical and biological ecosystem. Monitoring the patterns in freezing of lakes (including duration and extent of ice) can provide clues on climate change and global warming. This is recognized in the status of the Global Climate Observing System (task T10). In 2007, MeteoSwiss published the first national inventory of the most important climate observations in Switzerland, including observations of lake ice as part of the essential climate variable *lakes*. There exist already observations and data from local authorities, publications etc., however they are not systematic and come from different, uncoordinated and not secured sources. Traditionally, on-shore observers collected the information on lake ice, recording the visible ice-edge. Over the past two decades the number of field stations declined, due to lack of budget and/or human resources. Thus, MeteoSwiss initiated the project *integrated monitoring of ice in selected Swiss lakes* (Figures 1, 2) for an integrated multi-temporal monitoring of lake ice, using not only satellite images, but also exploring the possibilities of Webcams and in-situ measurements. The project aims to monitor a number of target lakes and detect the extent of ice and duration of lake ice, and in particular the freezing/thawing dates, with focus on the integration of various input data and processing methods. As part of this research, in this work, low spatial resolution ($250 - 1000$ m) but high temporal resolution (1 day) satellite images from MODerate-resolution Imaging Spectroradiometer (MODIS) sensors are used. Several spectral channels are utilized, both reflective and emissive (thermal). The target lakes include (in decreasing area from about 11.3 to 0.78 km^2): Sihl, Sils, Silvaplana, and St. Moritz. These lakes have variable area (very small to middle-sized), altitude (low to high) and surrounding topography (flat/hilly to mountainous). They freeze often, and cover medium to high difficulty cases for Alpine lakes (Table 1). The developed methods are expected to generalize to other similar or easier lake conditions in the Alps and beyond.

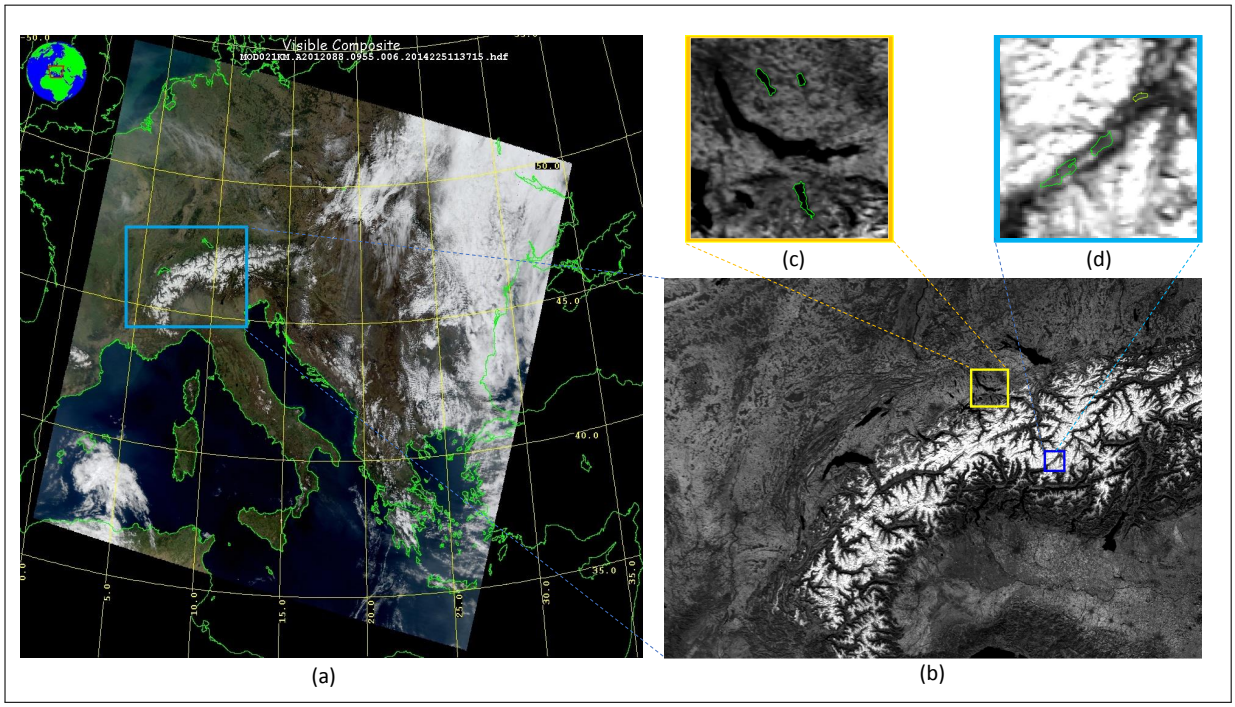

Figure 2. (a) Terra MODIS acquisition on 28 March 2012, 09 : 55 with region in and around Switzerland outlined in blue rectangle (b) MODIS band 2 (250m GSD) image covering region Switzerland and neighborhood with sub-regions around Zürich and Graubünden marked using yellow and violet rectangles respectively (c) Zoomed view of region around Zürich with green outlines around the target lakes Sihl (bottom), Greifen (top left) and Pfäffiker (top right) (d) Zoomed view of region around Graubünden with green outlines around the lake Sils (left), Silvaplana (middle) and St. Moritz (right).

Table 1. Characteristics of the four lakes being monitored.

	Lake Sihl	**Lake Sils**	**Lake Silvaplana**	**Lake St. Moritz**
Area (km^2)	11.3	4.1	2.7	0.78
Altitude (m)	889	1797	1791	1768
Freezing Frequency	medium	high	high	high

Our contributions. Firstly, we solved the problem of ice detection in selected Swiss lakes using MODIS satellite images with non-linear SVMs. Secondly, we have done a study to estimate the absolute geolocation accuracy of the MODIS sensor during the period of winter 2011-12. Thirdly, we have explored the recent algorithm by Lanaras et al. (2017) to super-resolve the low resolution channels to 250m, which effectively performs similar to bilinear interpolation.

2. RELATED WORK

Lake remote sensing. The potential of different remote sensing sensors covering varying time periods and spatial coverage to measure the occurrence of lake ice was demonstrated by several investigations (Maslanik and Barry, 1987, Palecki and Barry, 1986, Wynne and Lillesand, 1993). A comprehensive overview (Dörnhöfer and Oppelt, 2016) on the recent advances in lake remote sensing addresses lake ice phenology. The review and also focuses on lake properties such as water transparency, biota, water temperature and bathymetry. The survey primarily discusses challenges and potential advantages of lake ice monitoring using remote sensing data. The review suggests that even-though remote sensing techniques are unable to capture all indicators used in lake ecology, or to match the granularity of details as in-situ measurements, they certainly well support these sparsely distributed in-situ measurements with spatially and temporally more frequent data. Some studies on lake ice exist for Germany (Bernhardt et al., 2012), Austria and Hungary (Soja et al., 2014), as well as Spain (Sánchez-López et al., 2015).

MODIS-based approaches. For the region of southwest Alaska, inter-annual variation in the intensity and duration of lake ice, snow cover and vegetation index have been studied using MODIS imagery for the period 2001-2007 (Spencer et al., 2008). The work focused on 6 lakes and had an interesting conclusion that for a given lake, the ice-on dates varied in timing and duration, while the ice-off dates were more or less consistent. However, the percentage of

ice cover was interpreted manually, which clearly is a drawback when moving towards an operational system with repeatable results. On the other hand, an automated monitoring system (Tschudi et al., 2008) incorporated spectral unmixing of the MODIS surface reflectance product to derive the daily melt pond cover over sea ice in the Chukchi Sea region near Alaska for the summer of 2004. For the Arctic region, spectral unmixing was used to retrieve multi-annual data sets of melt pond fraction and sea ice concentration from MODIS data (Rösel et al., 2012). Three surface types: open water, melt ponds and snow and ice were distinguished. Artificial neural networks were also adopted to speed up the process. For the period 2000-2014, variations of annual Minimum Snow and Ice (MSI) extent over Canada and neighboring landmass were derived from MODIS 250m images (Trishchenko et al., 2016). Cooley and Pavelsky (2016) proposed an automated ice detection methodology from MODIS imagery which exposed spatial and temporal patterns in Arctic river ice breakup. This work explored the breakup timing on the Mackenzie, Lena, Ob and Yenisey rivers for the period 2000 till 2014. They also demonstrated that MODIS imagery could be used to differentiate thermal and mechanical breakup events. The MSI extent thus estimated showed fairly good consistency and was compared with the Randolph Glacier Inventory. In the recent past, a probabilistic approach was proposed for mapping landfast ice in the Canadian Arctic region using MODIS (Trishchenko et al., 2017). The approach is based on multi-temporal analysis of clear sky composites generated thrice a month from MODIS images. Pixel time serie are analyzed from April till September to produce the snow/ice flag. A probability is generated from these flag sequences, which is further utilized to analyze the landfast ice and its year-to-year variability.

Other satellite image-based approaches. Along with MODIS, Ice Mapping System (IMS) data was used to monitor daily ice cover changes in the lakes in Quebec region, Canada using a one-dimensional thermodynamic ice model (Brown and Duguay, 2012). The work concluded that MODIS outperforms IMS for estimation of ice-on due to finer resolution. Weber et al. (2016) used Advanced Very High Resolution Radiometer (AVHRR) satellite data to study ice phenology in the European lakes. An automated sensor-independent two-step extraction technique was proposed which utilized both near-infrared reflectance and infrared thermal values. Recently, Sütterlin et al. (2017) put forward a single-channel retrieval approach to detect lake phenology in Swiss lakes using the fine resolution I bands of the Visible Infrared Imaging Radiometer Suite (VIIRS) sensor on board Suomi National Polar-orbiting Partnership (NPP). Trishchenko and Ungureanu (2017) performed an inter-comparison of MODIS and VIIRS for mapping snow and ice extent over the Canadian landmass. The preliminary comparison performed for the period summer 2014 revealed that the rescaled VIIRS I-bands performed fairly close to the downscaled MODIS 250-m imagery. The difference in seasonal Minimum Snow/Ice (MSI) extent between VIIRS and MODIS was reported to be less than 0.4%.

3. DATA

Terra MODIS. MODIS is a passive imaging spectroradiometer with 490 detectors, arranged in 36 spectral bands that are sampled across the visible and infrared spectrum. The multi-spectral data is available in three different spatial resolutions 250m, 500m, and 1000m and temporal resolution of 1 day. In our analysis, we used the following three MODIS products: *MOD02:* the level 1B data set with calibrated and geolocated aperture radiances, *MOD03:* the geolocation product containing geodetic coordinates, ground elevation, solar and satellite zenith and azimuth angle, *MOD35:* the 48-bit fractional cloud mask product.

Useful MODIS channels. Either because of the presence of stripes or saturation, many channels of MODIS are not directly useful. Out of the 36 available channels, twelve were selected as possibly useful, through visual inspection. This set includes eight reflective (R) and four emissive (E) channels with different spatial resolutions. Details of the twelve selected channels are shown on Table 2.

Table 2. Spatial resolution (Res) and spectral bandwidth (BW) of the 12 potentially useful reflective (R) and emissive (E) MODIS spectral channels selected after visual inspection.

Band	b_1	b_2	b_3	b_4	b_6	b_{17}	b_{18}	b_{19}	b_{20}	b_{22}	b_{23}	b_{25}
Type	R	R	R	R	R	R	R	R	E	E	E	E
Res (m)	250	250	500	500	500	1000	1000	1000	1000	1000	1000	1000
BW (μm)	0.62 – 0.67	0.84 – 0.88	0.46 – 0.48	0.55 – 0.57	1.63 – 1.65	0.89 – 0.92	0.93 – 0.94	0.92 – 0.97	3.66 – 3.84	3.93 – 3.99	4.02 – 4.08	4.48 – 4.55

3.1 Super-Resolution

The different resolutions of the various MODIS bands pose the following challenge: a direct analysis of the data will deliver results at the lowest available resolution. A possible way around this problem is to infer the lower resolution bands in the highest available resolution. This procedure is usually termed *multispectral super-resolution* and is a generalization of pan-sharpening. The aim of these methods is to exploit the underlying information of all bands and obtain an image with high spatial and spectral resolution. This is possible by building on the assumption

that the discontinuities observed at the highest spatial resolution should be also present at lower resolutions. We thus take three different methods to increase the resolution of the 500m and 1000m bands to 250m; simple bilinear interpolation, ATPRK (Wang et al., 2015) and SupReME (Lanaras et al., 2017). ARTPK (area-to-point regression kriging) is a method that uses regression modeling to incorporate fine spatial resolution in the lower resolution bands. It does not have any important parameters to be set. However, it only accepts one high resolution input as either a single band or an average of the available high-res bands. The high resolution bands of MODIS (b_1 and b_2) are visually different and thus averaging them is not suitable. For ATPRK we only use b_2 as high-res input, because it lies in the NIR spectrum and it is especially useful for this lake application, as due to the properties of water the lake outlines are well visible. SupReME is a method that inverts the linear spectral mixing model, with adaptive, edge-preserving regularisation. It solves the inversion problem for all the bands simultaneously, and was applied with the following empirical parameter settings. The subspace dimension is set to $p = 7$, the spatial regularization as $\lambda = 0.2$ and the subspace weights $q = [1\ 1.5\ 8\ 15\ 15\ 20\ 20]$. An example with the 1000m resolution band b_{17} comparing the above methods is presented in Figure 3. As can be seen ATPRK and SupReME create sharper results than the bilinear interpolation. However, SupReME results in a smoother image without visible noise. Since there is no ground truth the results can only be judged qualitatively. For further processing, the bilinear interpolated and super-resolved with SupReME are used. We find empirically that we obtain better qualitative results if we only process the reflective bands (from the useful set). This is likely due to the fact that the emissive discontinuities do not fully coincide with the reflective ones, not fulfilling the assumption mentioned above. Thus, we run SupReME for all the dates in two configurations: including ($SupReME_{RE}$) and excluding ($SupReME_R$) the emissive bands in the processing.

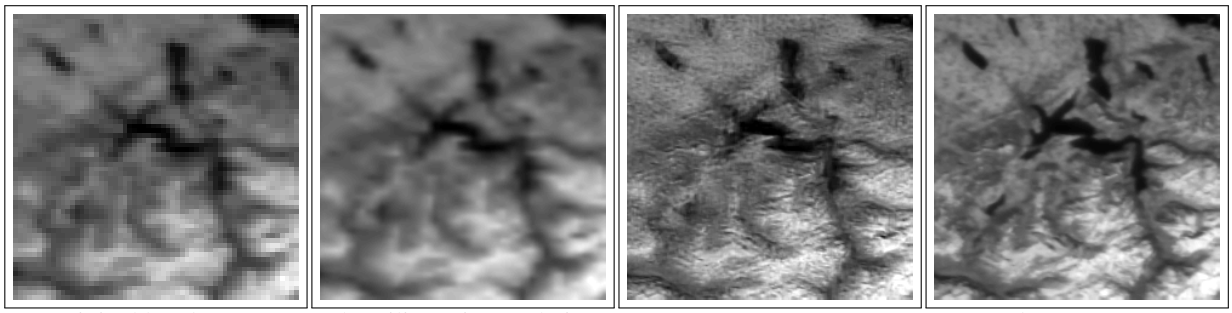

(a) Original band B_{17} 1KM (b) Bilinear interpolation (c) ATPRK (d) SupReME

Figure 3. Super-resolution example of reflective band b_{17}, showing a region with lakes in Switzerland. *Left*: the original 1000m band, *middle left*: the bilinearly interpolated band to 250m, *middle right*: the result of ATPRK, *right*: the result of SupReME.

4. METHODOLOGY

4.1 Pre-Processing

Cloud-mask generation. A further challenge of optical satellite image analysis is the lack of sufficient data. This issue is primarily due to occlusion by clouds. A binary cloud mask is derived from the MODIS 48-bit fractional cloud mask product. We follow a conservative approach and combine the *cloudy* and *uncertain clear* classes of the NASA product into a cloud mask. We used the *LDOPE* software tool provided by the MODIS land quality assessment group (Roy et al., 2002) to perform masking of bits and the *MRTSWATH* (MODIS Reprojection Tool Swath, n.d.) software to re-project to the reference UTM32N co-ordinate system. An example image and the derived binary mask are shown in Figure 4a and Figure 4b respectively. Each MODIS channel has 16-bit grey values of which the invalid pixels have value above 32767. These invalid pixels are also masked out. Only the cloud-free and valid pixels are processed further. The MODIS cloud masks are not perfect, still we rely on them for the moment and defer more accurate cloud masking to future work. For the moment, obvious mistakes (for instance very bright pixels on a lake in summer not marked as clouds) were removed manually before further analysis. Note also, the cloud mask is available only at a spatial resolution of 1000m. In order to process tha data at higher resolution (250m), the mask was upscaled with nearest neighbour interpolation.

Lake outline generation and absolute geolocation correction. The original outlines of the lakes were downloaded from `overpass-turbo.eu`. These outlines were further generalized by Douglas Peucker Algorithm (Douglas and Peucker, 1973). A comparison of the outlines pre- and post- generalization is shown in Figure 5. The generalized, digitized lake outlines are projected on to the images to guide the search and estimation of lake ice. We followed the approach by Aksakal (2013) to estimate and correct the absolute geolocation accuracy. Two dates per month were analyzed from December 2011 till March 2012. For this, we used many lakes, covering the whole area of Figure 2b. Fifteen lakes with a minimum area of 500 pixels (in 250m spatial resolution) in and around Switzerland were

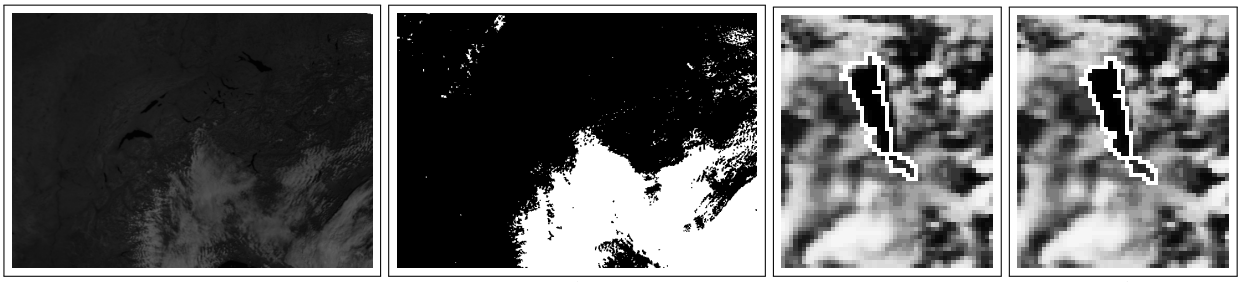

(a) (b) (c) (d)

Figure 4. (a) MODIS band 19 with 1000m GSD, (b) binary (*white*-cloudy, *black*-not cloudy) cloud mask combining the *cloudy* and *uncertain clear* categories, (c) Back-projected outline of lake Sihl (02.08.2012) before absolute geolocation correction, (d) after geolocation correction.

incorporated in the analysis. The analysis was performed only if the following two conditions were met : firstly, minimum 40% of each lake area should be cloud-free and secondly, large (partially) cloud-free lakes should exist in at least three out of four corners of the image. The results vary slightly among lakes as well as dates. For each date, the mean translational offsets in both x and y directions were computed by averaging, weighted by the number of cloud free pixels per lake. In the end, the average final shifts were computed. Final shifts were estimated as -0.75 pixel and -0.85 pixel in x and y directions respectively. Figure 4c and Figure 4d shows the back-projected outlines of lake Sihl before and after applying the correction of $+1$ pixel (approximated to the nearest integer value) each in x and y directions respectively.

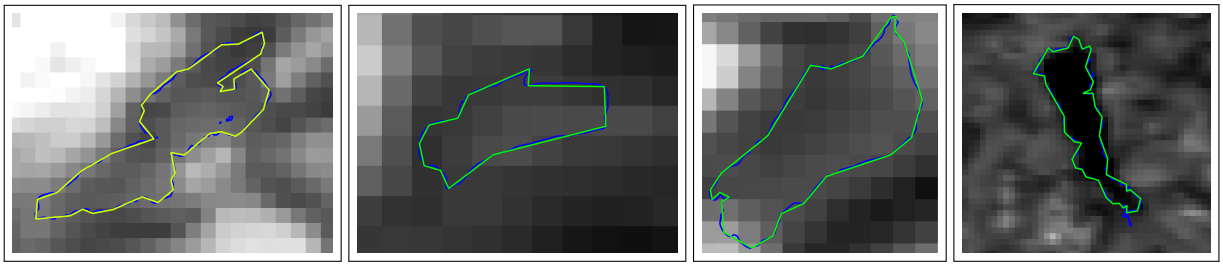

(a) Lake Sils (b) Lake St. Moritz (c) Lake Silvaplana (d) Lake Sihl

Figure 5. Comparison of original lake outlines (blue) and the generalized outlines (yellow). All the images are at 250m resolution but at different zoom levels for better visualization. Best viewed on screen.

Clean pixels vs. mixed pixels. All the pixels which lie completely inside the lake are termed as *clean*, pixels which only partially lie on the lake as *mixed*. The scope of this paper is limited to the analysis of clean pixels.

4.2 Grey Value Statistics

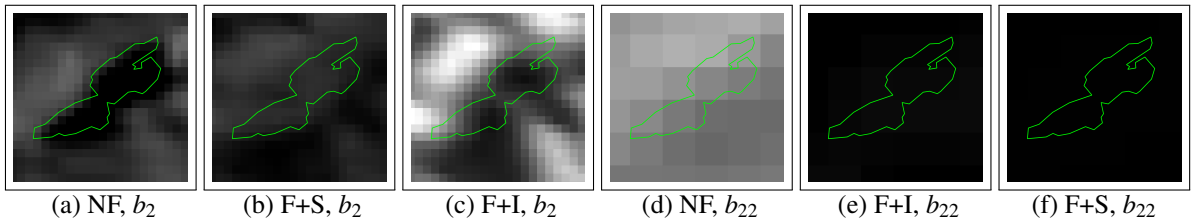

(a) NF, b_2 (b) F+S, b_2 (c) F+I, b_2 (d) NF, b_{22} (e) F+I, b_{22} (f) F+S, b_{22}

Figure 6. Lake Sils: comparison of lake pixel grey values for Non-Frozen (NF), Frozen and Ice (F+I), Frozen and Snow covered ice (F+S) on reflective band 2 (b_2, 250m GSD) and emissive band 22 (b_{22}, 1000m GSD). Best viewed on screen.

When a lake is frozen, the water can occur in two different states: firstly, the water freezes and appears as ice and secondly, snow falls and persists on top of the ice. We consider them as two separate sub-classes since the reflective and emissive properties of ice and snow are different. This difference is also reflected in the emissive and reflective spectral responses in different bands of the multi-spectral satellite images. An example for lake Sils is shown in Figure 6. For demonstration, band 2 (reflective, 250m resolution) and band 22 (emissive, 1000m resolution) are analyzed for 3 different cases: water, ice and snow on ice. Figure 6a shows that in band 2, the lake pixels appears to be darker when non-frozen (28.08.2012). On the other hand, Figure 6b illustrates that the pixels are brighter in band 2 when frozen and snow exists (06.02.2012). However, it can be observed from Figure 6c that the pixels are darker in band

2 when the lake is frozen, but not covered with snow (03.01.2012). This ice vs. water confusion can be overcome with the help of the emissive bands. Figures 6d, 6e and 6f shows that in emissive bands, the non-frozen pixels appear brighter as opposed to the frozen pixels (both snow and ice cases).

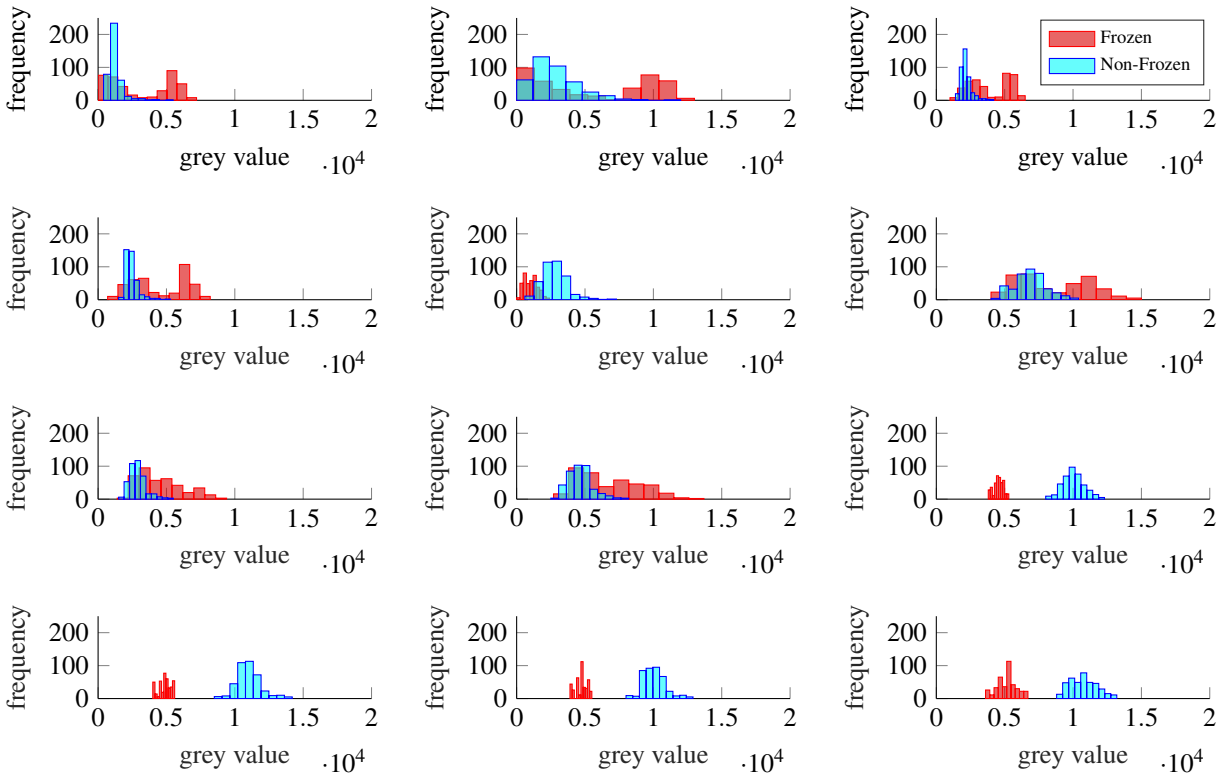

Figure 7. Frozen (Jan, Feb 2012) vs Non-Frozen (Jul, Aug 2012) statistics of clean cloud-free pixels in 12 selected MODIS channels for Lake Silvaplana. First row (b_1, b_2, b_3), second row (b_4, b_6, b_{17}), third row (b_{18}, b_{19}, b_{20}), fourth row (b_{22}, b_{23}, b_{25}).

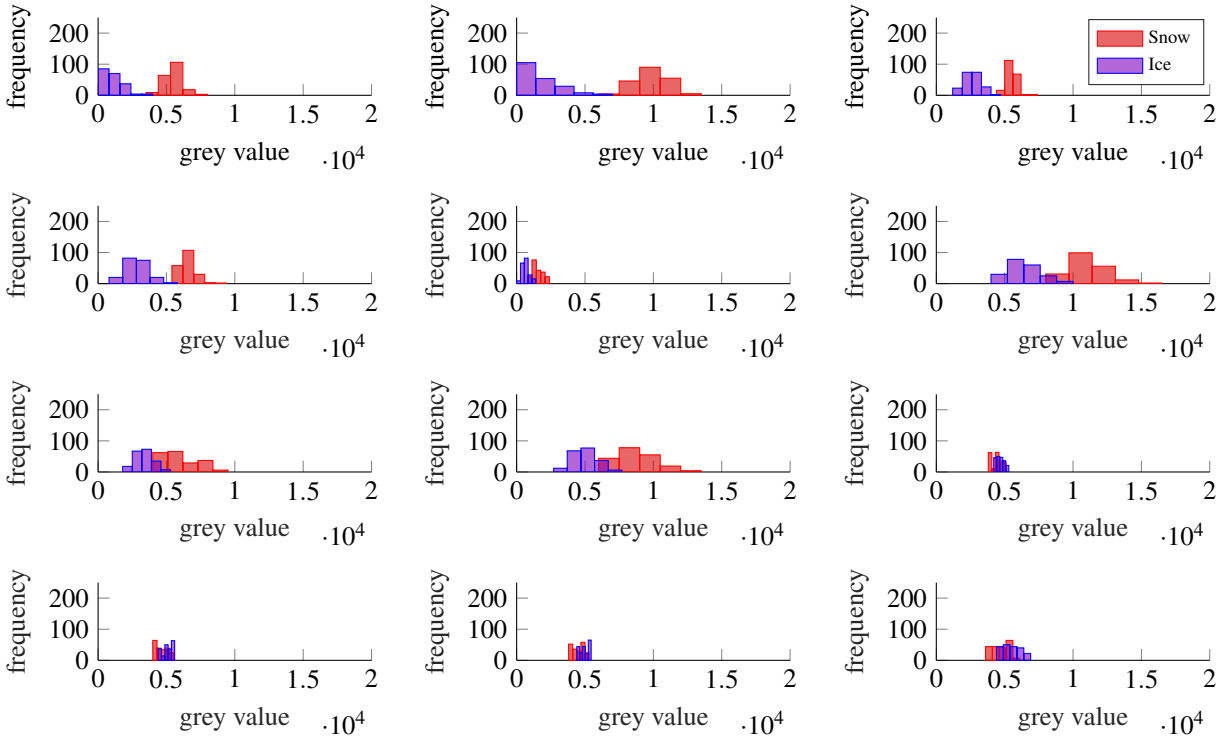

Figure 8. Snow vs Ice statistics of clean cloud-free pixels in 12 selected MODIS channels for Lake Silvaplana. First row (b_1, b_2, b_3), second row (b_4, b_6, b_{17}), third row (b_{18}, b_{19}, b_{20}), fourth row (b_{22}, b_{23}, b_{25}).

Table 3. Ground truth information on the cloud-free dates processed in 2012.

	Lake Sihl		Lake Sils		Lake Silvaplana		Lake St. Moritz	
	Period	**Days**	**Period**	**Days**	**Period**	**Days**	**Period**	**Days**
Frozen	06 - 25 Feb	7	Jan, Feb	23	Jan, Feb	23	Jan, Feb	23
Non-Frozen	Aug	13	Jul, Aug	26	Jul, Aug	21	Jul, Aug	22

Frozen vs. non-frozen pixels. The distributions of both frozen (January and February 2012) and non-frozen (July and August 2012) pixels in all the 12 selected bands of MODIS for lake Silvaplana are shown in Figure 7. It can be clearly seen that, the four emissive bands hold information to separate frozen and non-frozen pixels. Another important cue which can be observed from Figure 7 is that the distribution of frozen pixels especially in the first six reflective bands is bi-modal, probably one mode each from ice and snow pixels. To validate this bi-modal ice-snow hypothesis, the frozen data was relabeled as snow or ice based on visual interpretation. The respective distributions were computed for lake Silvaplana and are displayed in Figure 8. It is now evident that the cues to separate ice from snow are present in the reflective bands.

4.3 Semantic Segmentation

Out of the 12 probably useful spectral bands, the most significant channels to be used in the final feature vector were determined with the *xgboost* (Chen and Guestrin, 2016) technique. The result is shown in Figure 9. It can be observed that not all 12 channels are needed to separate frozen and non-frozen pixels. This result substantiates our observations from Figure 7.

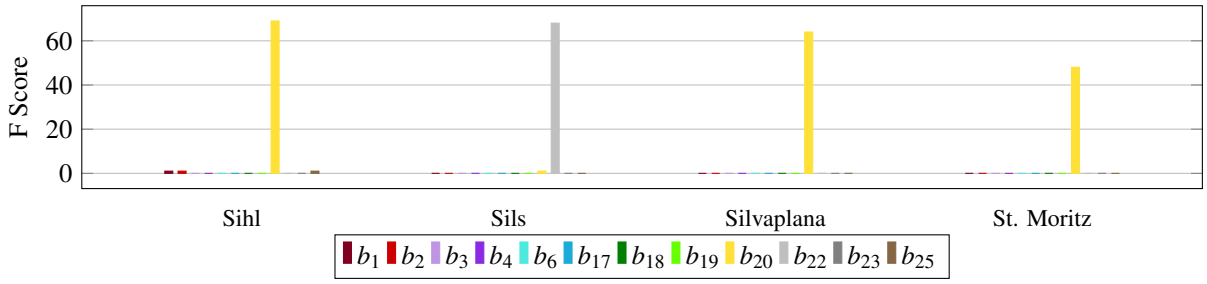

Figure 9. Bar graph showing the significance of each of the 12 channels for frozen vs non-frozen pixels separation using the *xgboost* algorithm. The dates displayed on Table 3 were used to select the frozen and non-frozen pixels.

We model the lake ice detection as a 2-class classification problem and use a non-linear Support Vector Machine (SVM) (Cortes and Vapnik, 1995) with Radial Basis Function (RBF) kernel. From Figure 9, we infer that the emissive channels are highly correlated and any one of them should be able to separate frozen pixels from their non-frozen counterparts, when fed into the SVM. The classifier is trained using only cloud-free *clean* pixels. Furthermore, we use SVM regression with the same kernel to estimate the probability for each pixel to be frozen. The probability is formed by feeding the regressor output through a sigmoid function.

5. RESULTS AND DISCUSSION

Ground truth. Human observations, media and police reports were used to determine the days on which the lakes were frozen. Ice cover changes gradually, so on some days lake can be only partially frozen. To ensure reliable reference data, we have in this work analyzed only the dates in which the lakes were completely frozen. The three target lakes in Graubünden region were definitely frozen during the first two months in 2012. However, lake Sihl was frozen for a lesser period. Details on the collected ground truth are listed on Table 3.

4-fold cross-validation. In k-fold cross-validation setup, the dataset will be randomly partitioned into k equal sized subsets. One of the k subsets will be used as test set, the remaining $k-1$ sets for training. This process is then repeated k times so that each data will be used for testing once. All experiments were 4-fold cross-validated, where the partitioning is done based on the date, to minimize temporal correlation between train and test folds.

5.1 Quantitative Results

Only the *clean* lake pixels were used to train the SVM model. Moreover, the classification results of only the *clean* pixels are taken into account for quantitative analysis. The *mixed* pixels have been ignored. Table 4 demonstrates that for all four target lakes, we obtain almost 100% classification accuracy with an SVM with RBF kernel. We have also

experimented with combinations of different MODIS bands as feature vectors and the results are presented on Table 4. In addition, we have done an experiment to study the efficacy of SupReME (Lanaras et al., 2017) super-resolution approach. For this, we used all 6 low-resolution reflective bands (b_3, b_4, b_6, b_{17}, b_{18}, b_{19}) as feature vectors after super-resolving them.

Table 4. Comparison of 4-fold cross-validated SVM results with different feature vectors and super-resolution strategies. $SupReME_{RE}$ and $SupReME_R$ respectively indicates the configurations including and excluding the emissive bands. The overall accuracy and kappa coefficients are both specified. The dates displayed on Table 3 were used in this analysis.

Feature	Super Resolution	Sihl		Sils		Silvaplana		St. Moritz	
		accuracy	kappa	accuracy	kappa	accuracy	kappa	accuracy	kappa
b_2	Bilinear	98.04%	0.953	77.03%	0.517	73.79%	0.488	86.6%	0.731
all 12 *bands*	Bilinear	94.21%	0.868	98.63%	0.973	99.23%	0.985	96.65%	0.932
$b_{3,4,6,17,18,19}$	Bilinear	99.56%	0.991	99.32%	0.986	99.78%	0.996	97.77%	0.955
$b_{3,4,6,17,18,19}$	$SupReME_{RE}$	94.35%	0.875	99.80%	0.996	**100.0%**	**1.0**	98.88%	0.978
$b_{3,4,6,17,18,19}$	$SupReME_R$	**100.0%**	**1.0**	98.56%	0.971	99.56%	0.991	98.32%	0.966
b_{22}	Bilinear	**100.0%**	**1.0**	**100.0%**	**1.0**	**100.0%**	**1.0**	**100.0%**	**1.0**
$b_{2,22}$	Bilinear	**100.0%**	**1.0**	**100.0%**	**1.0**	**100.0%**	**1.0**	**100.0%**	**1.0**

In the analysis till now, we have collected non-frozen data from the months July and August 2012 (Table 3) which are rather less challenging as opposed to non-frozen dates from March 2012 (Sihl) and November 2011 (Sils, Silvaplana, St. Moritz). In order to double-check our results, we have also experimented with these challenging non-frozen dates, while the frozen dates remains the same. The results are displayed on Table 5 where the bands 2 (reflective) and 22 (emissive) were used to form the feature vector after standardization. Bands 2 and 22 originally have 250m and 1000m resolutions respectively. Band 22 was super-resolved to 250m resolution prior to analysis. Different super-resolution methodologies are also compared.

Table 5. Comparison of 4-fold cross-validated SVM results on challenging dates with different super-resolution strategies. $SupReME_{RE}$ indicates the configuration including the emissive bands.

Feature	Super Resolution	Sihl		Sils		Silvaplana		St. Moritz	
		accuracy	kappa	accuracy	kappa	accuracy	kappa	accuracy	kappa
b_{22}	Bilinear	**98.64%**	**0.973**	**98.12%**	**0.961**	95.96%	0.915	92.57%	0.844
b_{22}	$SupReME_{RE}$	95.74%	0.917	95.40%	0.904	90.76%	0.808	97.30%	0.944
$b_{2,22}$	Bilinear	95.10%	0.894	97.85%	0.956	**99.94%**	**0.998**	**100.0%**	**1.0**
$b_{2,22}$	$SupReME_{RE}$	97.89%	0.956	96.68%	0.925	94.74%	0.891	95.95%	0.916

Effect of SupReME. It can be inferred from Table 4 and 5 that the results of SupReME are comparable with bilinear interpolation. $SupReME_R$ performs slightly better than $SupReME_{RE}$ for lake ice detection because the reflective and thermal edges are different.

5.2 Qualitative Results

Qualitative results are presented in Figure 10. The first column displays the area near the lake with the outlines overlaid. The respective cloud masks are shown in the second column, with cloudy pixels indicated in green. The third column displays the pixel-wise probability for being frozen, as derived from SVM regression. The more red the pixel means the more probable to be frozen. The final column delineates the pixel-wise classification results with red and black being frozen and non-frozen respectively. The first row shows the test case when lake Sihl was frozen while the second row when non-frozen. The third and fourth rows displays the results when lake Sils was frozen and non-frozen respectively.

6. CONCLUSIONS AND FUTURE WORK

In this paper, we have tackled lake ice detection as a pixel-wise, two-class semantic segmentation problem. We have used only MODIS images and processed them with standard non-linear SVM classification. The most useful MODIS channels to solve the problem, as determined with *xgboost*, turn out to be the reflective b_2 channel and the emissive b_{22} channel. We have analyzed four different lakes in Switzerland, and obtain near-perfect results in distinguishing

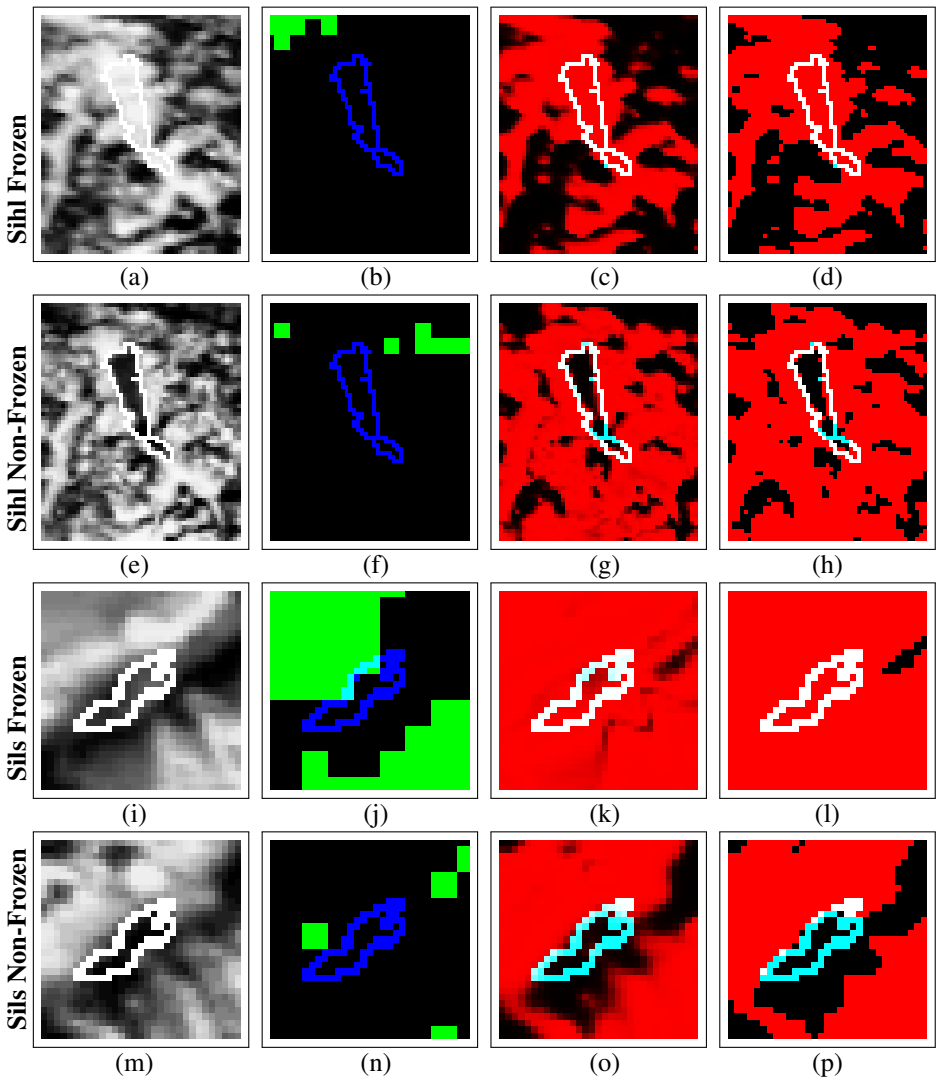

Figure 10. (*a, e, i, m*) Histogram equalized image of band b_2 in and around the lake, (*b, f, j, n*) Cloud-mask indicating cloudy pixels in green, (*c, g, k, o*) Confidence measure from SVM regression where the more red the pixel the more probable to be frozen, (*d, h, l, p*) SVM classification result indicating pixels predicted as frozen in red and non-frozen in black.

frozen pixels from their non-frozen counterparts. Our results can be directly applied to other lakes with similar conditions, in Switzerland as well as other regions. In the paper, we have limited the analysis to *clean* pixels, which lie completely inside the lake. In future work, we plan to extend our approach to incorporate the *mixed* pixels, and include a larger range of more lakes and dates in the analysis.

ACKNOWLEDGEMENTS

This work is part of the project *Integrated Monitoring of Ice in Selected Swiss Lakes* funded by Swiss Federal Office of Meteorology and Climatology MeteoSwiss in the framework of GCOS Switzerland.

REFERENCES

Aksakal, S. K., 2013. Geometric accuracy investigations of SEVIRI high resolution visible (HRV) level 1.5 imagery. Remote Sensing 5(5), pp. 2475–2491.

Bernhardt, J., Engelhardt, C., Kirillin, G. and Matschullat, J., 2012. Lake ice phenology in Berlin-Brandenburg from 1947-2007: observations and model hindcasts. Climatic Change 112(3), pp. 791–817.

Brown, L. C. and Duguay, C. R., 2012. Modelling lake ice phenology with an examination of satellite-detected subgrid cell variability. Advances in Meteorology 6(2), pp. 431–446.

Chen, T. and Guestrin, C., 2016. Xgboost: A scalable tree boosting system. In: Proceedings of the 22nd ACM SIGKDD International Conference on Knowledge Discovery and Data Mining, San Francisco, California, USA, pp. 785–794.

Cooley, S. W. and Pavelsky, T. M., 2016. Spatial and temporal patterns in arctic river ice breakup revealed by automated ice detection from modis imagery. Remote Sensing of Environment 175, pp. 310–322.

Cortes, C. and Vapnik, V., 1995. Support-vector networks. Machine Learning 20(3), pp. 273–297.

Dörnhöfer, K. and Oppelt, N., 2016. Remote sensing for lake research and monitoring - Recent advances. Ecological Indicators 64, pp. 105–122.

Douglas, D. H. and Peucker, T. K., 1973. Algorithms for the reduction of the number of points required to represent a digitized line or its caricature. Cartographica: The International Journal for Geographic Information and Geovisualization 10(2), pp. 112–122.

Lanaras, C., Bioucas-Dias, J., Baltsavias, E. and Schindler, K., 2017. Super-resolution of multispectral multiresolution images from a single sensor. In: IEEE CVPR Earth Vision Workshop, Honolulu, Hawaii, USA.

Maslanik, J. A. and Barry, R. G., 1987. Lake ice formation and breakup as an indicator of climate change: Potential for monitoring using remote sensing techniques. The influence of climate change and climatic variability on the hydrologic regime and water resources (Proceedings of the Vancouver Symposium) IAHS publication no.(168), pp. 153–161.

MODIS Reprojection Tool Swath, n.d. Retrieved September 01, 2017, from `https://lpdaac.usgs.gov/tools/modis_reprojection_tool_swath`.

Palecki, M. A. and Barry, R. G., 1986. Freeze-up and break-up of lakes as an index of temperature changes during the transition seasons: a case study for Finland. Journal of Climate and Applied Meteorology 25(7), pp. 893–902.

Rösel, A., Kaleschke, L. and Birnbaum, G., 2012. Melt ponds on Arctic sea ice determined from MODIS satellite data using an artificial neural network. Cryosphere 6(2), pp. 431–446.

Roy, D., Borak, J., Devadiga, S., Wolfe, R., Zheng, M. and Descloitres, J., 2002. The MODIS land product quality assessment approach. Remote Sensing of Environment 83, pp. 62–76.

Sánchez-López, G., Hernndez, A., Pla-Rabes, S. and Toro, M., 2015. The effects of the NAO on the ice phenology of Spanish alpine lakes. Climatic Change 130(2), pp. 101–113.

Soja, A. M., Kutics, K., Maracek, K., Molnr, G. and Soja, G., 2014. Changes in ice phenology characteristics of two central European steppe lakes from 1926 to 2012 - Influences of local weather and large scale oscillation patterns. Climatic Change 126(1-2), pp. 119–133.

Spencer, P., Miller, A. E., Reed, B. and Budde, M., 2008. Monitoring lake ice seasons in southwest Alaska with MODIS images. In: Pecora 17 Conference: The Future of Land Imaging Going Operational, Denver, Colorado, USA.

Sütterlin, M., Duguay-Tetzlaff, A. and Wunderle, S., 2017. Toward a lake ice phenology derived from VIIRS data. In: EGU General Assembly, Vienna, Austria.

Trishchenko, A. P. and Ungureanu, C., 2017. Intercomparison of MODIS and VIIRS results for mapping summer minimum of snow and ice (msi) extent over Canadian landmass. In: 8th EARSeL workshop on Land Ice and Snow, Bern, Switzerland.

Trishchenko, A. P., Kostylev, V. and Whalen, D., 2017. Probabilistic approach for mapping landfast and sea ice extent in the Canadian Arctic Archipelago from MODIS at 250m spatial resolution. In: 8th EARSeL workshop on Land Ice and Snow, Bern, Switzerland.

Trishchenko, A. P., Leblanc, S. G., Wang, S., Li, J., Ungureanu, C., Luo, Y., Khlopenkov, K. V. and Fontana, F., 2016. Variations of annual minimum snow and ice extent over Canada and neighboring landmass derived from MODIS 250-m imagery for 2000-2014. Canadian Journal of Remote Sensing 42(3), pp. 214–242.

Tschudi, M. A., Maslanik, J. A. and Perovich, D. K., 2008. Derivation of melt pond coverage on Arctic sea ice using MODIS observations. Remote Sensing of Environment 112(5), pp. 2605–2614.

Wang, Q., Shi, W., Atkinson, P. M. and Zhao, Y., 2015. Downscaling MODIS images with area-to-point regression kriging. Remote Sensing of Environment 166, pp. 191–204.

Weber, H., Riffler, M., Nõges, T. and Wunderle, S., 2016. Lake ice phenology from AVHRR data for European lakes: An automated two-step extraction method. Remote Sensing of Environment 174, pp. 329–340.

Wynne, R. H. and Lillesand, T. M., 1993. Satellite observation of lake ice as a climate indicator: Initial results from statewide monitoring in Wisconsin. Photogrammetric Engineering and Remote Sensing 59(6), pp. 1023–1031.